Reentrant spin-glass state and magnetodielectric effect in the spiral magnet BiMnFe$_2$O$_6$

Somnath Ghara,[1] Byung-Gu Jeon,[2] Kyongjun Yoo,[2] Kee Hoon Kim,[2] and A. Sundaresan[1,*]

[1]*Chemistry and Physics of Materials Unit and International Centre for Materials Science,*

Jawaharlal Nehru Centre for Advanced Scientific Research, Jakkur P.O., Bangalore 560064, India

[2]*CeNSCMR, Department of Physics and Astronomy, Seoul National University, Seoul 151-747, Republic of Korea*

The complex oxide BiMnFe$_2$O$_6$ crystallizing in a centrosymmetric orthorhombic structure ($Pbcm$) is known to exhibit a spiral antiferromagnetic ordering at $T_N \sim 212$ K and an anomaly in magnetization at low temperature ($T_P \sim 34$ K). To understand the origin of the low temperature anomaly and to verify experimentally whether or not the spiral magnetism induces ferroelectricity, we have carried out detailed magnetization and electrical measurements on a polycrystalline sample. Frequency-dependent ac susceptibility, dc magnetic memory effect, and dc magnetization relaxation studies show that the low temperature anomaly at T_P is associated with a reentrant spin-glass transition. From dc magnetization, we found that there exists another distinct temperature (T_{irr}), which corresponds to a strong thermomagnetic irreversibility. The field dependence of these two temperatures, $T_P(H)$ and $T_{\mathrm{irr}}(H)$, follow Gabay-Toulouse and de Almeida–Thouless lines, respectively, which are indicative of the Heisenberg spin-glass state. We also observe another magnetic anomaly at $T^* \sim 170$ K, where a dielectric anomaly with a significant magnetocapacitance effect is observed. However, pyroelectric current and positive-up-negative-down measurements reveal the absence of ferroelectricity in this compound.

I. INTRODUCTION

Magnetoelectric multiferroic materials, in which certain types of magnetic ordering induce ferroelectricity, have received much attention because of their large magnetoelectric coupling compared to those materials where ferroelectricity and magnetism have different origins [1–4]. A typical example is the perovskite oxide TbMnO$_3$, which has a centrosymmetric orthorhombic structure ($Pbnm$) and therefore does not exhibit ferroelectricity at room temperature. It undergoes a collinear sinusoidal antiferromagnetic ordering at 41 K due to magnetic frustration arising from nearest neighbor ferromagnetic and next nearest neighbor antiferromagnetc interactions. At $T_C \sim 28$ K, the spin structure changes into a noncollinear cycloidal arrangement that breaks the inversion symmetry and renders this material multiferroic [5]. Similar results were reported for CuO [6], MnWO$_4$ [7], Ni$_3$V$_2$O$_8$ [8], and several other oxides, all of which indeed exhibit a cycloidal magnetic ordering. In all these materials, the origin of ferroelectric polarization is explained by the spin-current model or inverse Dzyaloshinskii-Moriya (DM) interaction [9]. This model is also applicable to materials such as the spinel CoCr$_2$O$_4$ [10] and the Y-type hexaferrite Ba$_2$Mg$_2$Fe$_{12}$O$_{22}$ [11] exhibiting a transverse-conical spin arrangement. Thus, noncollinear spiral magnetic ordering seems to be a key in exploring new materials for multiferroic properties. It is known that certain collinear magnetic ordering also induces ferroelectricity [1].

Recently, a complex oxide, BiMnFe$_2$O$_6$, having two potential mechanisms for ferroelectricity, namely, the stereoactive Bi^{3+} ion and a spiral antiferromagnetic ordering ($T_N \sim 212$ K) of Mn^{3+}/Fe^{3+} ions, has been reported [12]. However, both these mechanisms do not seem to induce ferroelectricity in this compound [12,13]. Consistent with the centrosymmetric structure ($Pbcm$), the polar Bi^{3+} ions are arranged in an

antiferroelectric manner and thus produce no ferroelectricity [13]. On the other hand, a disorder arrangement of magnetic ions in two different crystallographic sites results in frustrated magnetic interactions that lead to a long-range spiral magnetic ordering which remains down to low temperatures (7 K). Based on the analysis of neutron diffraction data and density functional theory calculations, it has been shown that the spiral spins lying in the ac plane propagate along the b axis, but a strong antiferromagnetic coupling of spiral chains along the c axis makes this material nonpolar [12]. At low temperatures, a magnetic anomaly was observed at $T_P \sim 34$ K, which has been attributed to a possible magnetic phase separation [13].

Here, we have carried out detailed magnetic and electrical measurements to understand the low temperature magnetic anomaly and to verify the proposed nonpolar state. Our study suggests that the magnetic peak at $T_P \sim 34$ K is associated with a reentrant spin-glass transition. Further, we observe a magnetic and dielectric anomaly at a temperature ($T^* \sim 170$ K) that is lower than the spiral antiferromagnetic ordering ($T_N \sim 212$ K). A significant magnetocapacitance effect is observed around this anomaly. Pyroelectric current and P-E measurements based on the positive-up-negative-down (PUND) method suggest that the magnetic and dielectric anomalies are not associated with ferroelectricity.

II. EXPERIMENT

A polycrystalline sample of BiMnFe$_2$O$_6$ was prepared by the solid state reaction method. Stoichiometric amounts of the starting materials Bi$_2$O$_3$, Mn$_2$O$_3$, and Fe$_2$O$_3$ were mixed and heated at 900 °C with several intermediate grindings. The phase purity was checked by analyzing x-ray diffraction data collected with the PANalytical Empyrean alpha-1 diffractometer using monochromatized Cu $K\alpha_1$ radiation [14]. A structural analysis was carried out by the Rietveld refinement method using FULLPROF software [15,16]. Magnetic measurements were made with a superconducting quantum
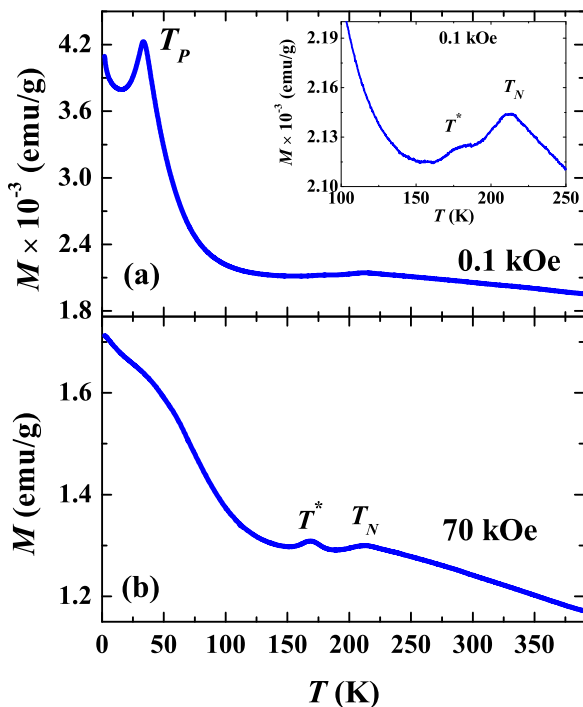
———————
*sundaresan@jncasr.ac.in

FIG. 1. (Color online) Temperature-dependent field-cooled (FC) magnetization under applied fields of (a) 0.1 kOe and (b) 70 kOe, respectively. Magnified view of FC magnetization under an applied field of 0.1 kOe is shown in the inset of (a), where the magnetic anomaly around 170 K can be seen clearly.

interference device (SQUID) magnetometer in both the vibrating sample and dc scan mode. ac susceptibility measurements were made with the physical property measurement system (PPMS, Quantum Design). Electrodes were made with silver paste for electrical measurements. The pyroelectric current and capacitance were measured with an electrometer (Keithley 6517A) and an *LCR* meter (Agilent E4980A), respectively, using a multifunctional probe inside the PPMS. Pyroelectric current measurements were made by cooling the sample in an electric field from 200 to 50 K, and, after removing the field, the sample was shortened for a long time to remove stray charges, and then the pyrocurrent was recorded during warming. The conventional *P*-*E* loop and PUND measurements were performed with a Radiant Technology precision workstation and a home-made circuit based on the Sawyer-Tower circuit, respectively [17,18].

III. RESULTS AND DISCUSSION

A. dc magnetization

The temperature dependence of field-cooled magnetization under an applied magnetic field of 0.1 kOe is shown in Fig. 1(a). As reported earlier [13], we observe two anomalies in magnetization, one at $T_N \sim 212$ K and another at low temperature ($T_P \sim 34$ K). In addition to these two magnetic peaks (at T_N and T_P), we also observe a weak magnetic anomaly at $T^* \sim 170$ K at a low field (0.1 kOe), as shown in the inset of Fig. 1(a). This anomaly, which was unnoticed in an earlier study [13], can be seen clearly at higher magnetic fields, as shown for an applied field of 70 kOe in Fig. 1(b).
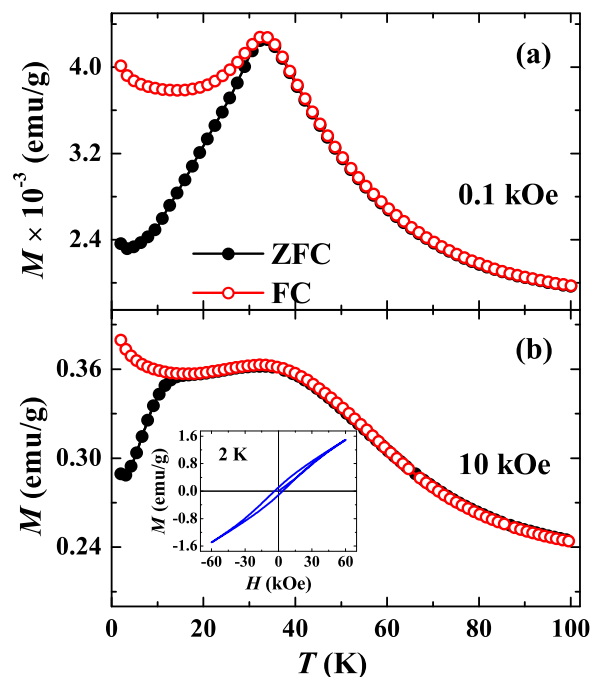

FIG. 2. (Color online) Temperature-dependent zero-field-cooled (ZFC) and field-cooled (FC) magnetization under an applied field of (a) 0.1 kOe and (b) 10 kOe, respectively. *M* vs *H* at 2 K is shown in the inset of (b).

Though the long-range magnetic ordering occurs at $T_N \sim$ 212 K, the magnetic susceptibility follows the Curie-Weiss law only above 450 K. This is consistent with the presence of a short-range magnetic interaction above T_N, as indicated by the neutron diffraction study. The effective paramagnetic moment (μ_{eff}) obtained from the fit is $9.89\mu_B$, which is close to the theoretical value ($9.69\mu_B$). The obtained value of the Curie-Weiss temperature (θ_{CW}) is -890 K, which is much higher than T_N, indicating the presence of magnetic frustration. The frustration parameter f ($=-\theta_{\text{CW}}/T_N$) is found to be 4.2, which suggests that the system is moderately frustrated [19].

Field-cooled (FC) and zero-field-cooled (ZFC) magnetizations with 0.1 and 10 kOe magnetic fields are shown in Figs. 2(a) and 2(b), respectively. Both the FC and ZFC magnetization curves show a peak around 34 K (T_P) and bifurcate below a temperature (T_{irr}), which is the onset of thermomagnetic irreversibility (TMI). These two temperatures (T_{irr} and T_P) depend strongly on the applied magnetic field. In typical Heisenberg spin-glass systems, two different lines corresponding to a strong and weak irreversibility temperature have been observed in the H-T phase diagram, which are known as the de Almeida–Thouless (AT) line and Gabay-Touelouse (GT) line, respectively [20,21]. For the present system, we found that $T_{\text{irr}}(H)$ and $T_P(H)$ follow the AT line and GT line, respectively. These two lines can be represented by a general equation,

$$T_{\text{irr},P}(H) = T_{\text{irr},P}(0)(1 - CH^n),$$

where C is a constant and $T_{\text{irr},P}(0)$ is the T_{irr} and T_P at zero magnetic field. Theoretically, for the AT line, $n = \frac{2}{3}$, and for the GT line, $n = 2$. The experimental data of $T_{\text{irr}}(H)$ are fitted
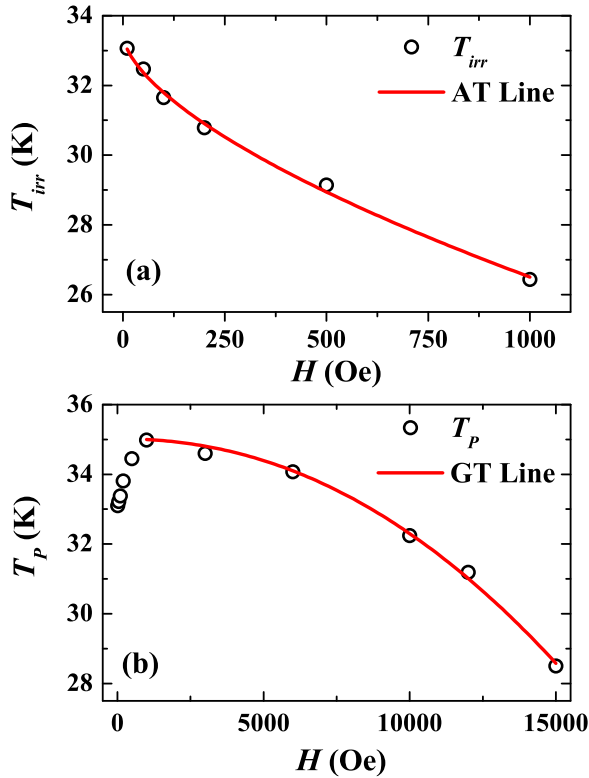
FIG. 3. (Color online) Dependence of (a) irreversibility temperature (T_{irr}) and (b) low temperature peak position (T_P) of magnetization as a function of magnetic field. AT and GT lines are shown by solid lines.
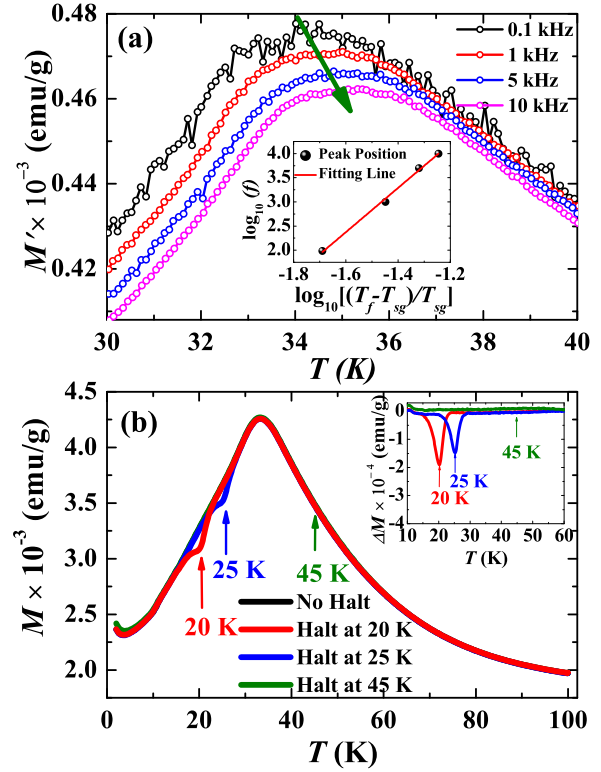

FIG. 4. (Color online) (a) Temperature-dependent real part of ac susceptibility with different frequencies. The inset curve shows a critical slowing down behavior of peak position T_f. (b) dc memory effect experiments performed without halt and with halt at three different temperatures, $T_W = 20$, 25, and 45 K, in the zero-field-cooled mode. The inset shows the difference in magnetization ΔM ($= M_{\text{with halt}} - M_{\text{without halt}}$) between without halt and with halt ZFC magnetization.

with the above relation and the result is shown in Fig. 3(a). It is found that a best fit can be obtained only at a low field region ($H < 1000$ Oe) [14]. The value of $T_{\text{irr}}(0)$ obtained from the fit is 33.4 K and the value of n is 0.62 (± 0.06), which is close to the theoretical value of n ($= \frac{2}{3}$) for the AT line for a spin-glass system [20]. On the other hand, the dependence of T_P on magnetic field is quite unusual, as shown in Fig. 3(b). With increasing magnetic field, the T_P increases initially, and above a critical field it decreases and follows the Gabay-Thouless (GT) line [21]. The value of n obtained from fitting $T_P(H)$ data with the above equation is 2.12 (± 0.09), which is almost equal to the theoretical value of $n = 2$ for spin-glass systems. The initial increase of $T_P(H)$ data at low fields may arise from uniaxial anisotropy, as suggested in La$_{0.9}$Sr$_{0.1}$CoO$_3$ [22]. It could also be due to the effect of applied field on the spiral spin structure. The bifurcation between ZFC and FC magnetization and the presence of AT and GT lines in the H-T phase diagram are an indication of the Heisenberg (reentrant) spin-glass state below 34 K. Similar behavior has been observed in many spin-glass systems [22–26]. It should be noticed that the field-dependent isothermal magnetization data at 2 K [inset of Fig. 2(b)] shows a hysteresis loop which is similar to that of typical spin-glass systems [27].

B. ac susceptibility

In order to further explore the presence of glassy behavior, we have carried out ac susceptibility, dc memory, and relaxation measurements. Figure 4(a) shows the real part of

ac susceptibility, where it can be seen that the peak position, which is known as the freezing temperature (T_f), shifts to a high temperature with increasing frequency of the applied ac magnetic field. This result confirms the presence of a spin-glass state at a temperature well below the long-range spiral antiferromagnetic ordering, and thus confirms a reentrant spin-glass state [27]. We further analyzed ac susceptibility data to get more insight into the nature of the glassy state. The frequency-dependent peak shift is defined by a parameter (S) [27], which is given by

$$S = \frac{\Delta T_f}{T_f \{\Delta \log_{10}(f)\}},$$

where $\Delta T_f = T_{f_1} - T_{f_2}$ and $\Delta \log_{10}(f) = \log_{10} f_1 - \log_{10} f_2$. This parameter is used to distinguish the spin-glass state from the superparamagnetic state. For a spin-glass system, S should satisfy $0.005 < S < 0.08$, and for a superparamagnetic state, $S > 0.2$ [27]. The obtained value of S for this system is 0.0175, which suggests that the glassy state is due to a (reentrant) spin-glass transition. It is well known that T_f follows a critical slowing down behavior [27–29], which is given by the following equation,

$$\tau = \tau_0 \left(\frac{T_f - T_{\text{SG}}}{T_{\text{SG}}} \right)^{-z\nu},$$

where τ is the characteristic time corresponding to excitation frequency f, T_{SG} is the freezing temperature at $f = 0$ Hz, τ_0 is a characteristic time constant which is related to the spin-flipping time, and $z\nu$ is a dynamical critical exponent. In the inset of Fig. 4(a), $\log_{10} f$ vs $\log_{10}[(T_f - T_{SG})/T_f]$ is plotted which can be fitted well with the above critical slowing down equation with $T_{SG} = 33.4$ K, which is the same as $T_{irr}(0)$ obtained from the fitted de Almeida–Thouless line. The values of τ_0 and $z\nu$ obtained from the best fit to a straight line are 3.147×10^{-11} s and 4.58, respectively. For a spin-glass system, τ_0 and $z\nu$ are typically $\sim 10^{-12}$–10^{-13} s and 4–12, respectively [24,30]. These results indicate the presence of a spin-glass state at low temperature. However, the value of τ_0 is one order higher than that of a typical spin-glass system but smaller than that of a typical cluster glass system ($\sim 10^{-7}$–10^{-10} s) [24,30]. This indicates that there may be some interacting spin-cluster phase below the reentrant spin-glass transition.

C. Memory and relaxation

Memory and rejuvenation effects are important characteristics of a spin-glass system [31–33]. A dc magnetic memory effect experiment was performed in the following way [34]: The sample was cooled to a particular temperature (T_W) in a ZFC condition where the sample is allowed to wait for a duration of $t_w = 6000$ s. Then the sample is cooled to a lowest possible temperature, and magnetization is recorded during warming in the presence of a 0.1 kOe magnetic field. Figure 4(b) shows the ZFC magnetization without halt and with halt at three different temperatures, $T_W = 20$, 25, and 45 K. The magnetization shows a clear dip at the waiting temperature ($T_W = 20$ and 25 K) when the waiting temperature is less than T_P. This memory effect is clearly observed in the inset figure where $\Delta M = M_{ZFC(with\ halt)} - M_{ZFC(without\ halt)}$ is plotted. Such a dip is not observed when T_W is above T_P. These memory effect experiments clearly indicate the presence of a metastable glassy state below T_P.

Magnetization relaxation experiments are performed by measuring the time-dependent magnetization at different temperatures below 34 K after cooling the sample under FC conditions with a 0.1 kOe field, and data were recorded after switching off the field to zero. In Fig. 5(a), normalized magnetization $m(t)$ $(=M_t/M_{t=0})$ is plotted as a function of time (t). The $m(t)$ versus time data of all temperatures below 34 K can be fitted well with the stretched exponential equation [35–38], which is given by

$$m(t) = m_0 - m_g \exp\left[-\left(\frac{t}{\tau}\right)^\beta\right],$$

where τ is the characteristic relaxation time constant, β is the stretching exponent, m_g is related to a glassy component of magnetization, and m_0 is related to an initial remnant magnetization which is required to fit the decay of magnetization of reentrant spin-glass systems. For a spin-glass system, β remains in the range $0 < \beta < 1$. From the fitting, the obtained value of β remains in between 0.42 and 0.51. The value of the relaxation time constant depends on temperature. It decreases
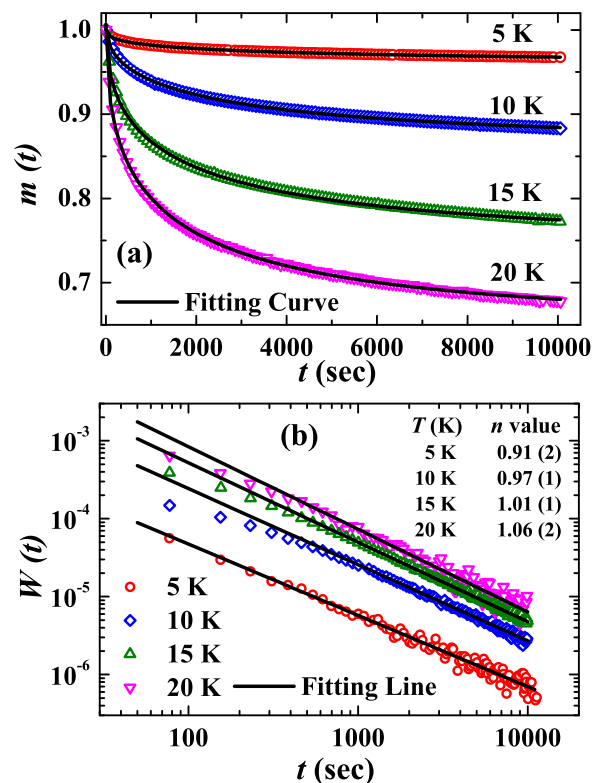

FIG. 5. (Color online) (a) Relaxation of field-cooled (FC) magnetization $m(t) = M_t/M_{t=0}$ at 5, 10, 15, and 25 K. Solid lines represent the stretched exponential fitting curve. (b) $W(t) = -\frac{d}{dt}[\ln m(t)]$ vs time at 5, 10, 15, and 20 K. Solid lines represent the fitting line with the $W(t) = At^{-n}$ equation.

continuously from 3584 s (at 5 K) to 1347 s (at 20 K) with increasing temperature.

To know whether or not the temperature dependence of relaxation time constant is coupled to the presence of an interacting cluster, we have followed the model proposed by Ulrich [39]. According to this model, after a crossover time, the rate of change of normalized thermoremnant magnetization $m(t)$, defined by $W(t) = -\frac{d}{dt}[\ln m(t)]$, of a system of magnetic particles, should decay with time as a power law [$W(t) \sim At^{-n}$] [39]. The value of n is very important and depends on the density of the particles and interaction between them. For a real spin-glass system, the values of n should remain constant throughout the temperature below the spin-glass transition. For this system, the $W(t)$ versus time plot at different temperatures is shown in Fig. 5(b). We find that the value of n increases continuously from 0.91 to 1.06 with an increase in temperature from 5 to 20 K. This analysis strongly indicates that the glassy state is not a simple atomic spin glass; it includes some strongly interacting spin clusters as well. Therefore, the glassy state in the present system may be termed as a reentrant spin-cluster glass. Using this model, a similar spin-cluster glass state was proposed in manganites and cobaltites [40–42].

All these results suggest that long-range magnetic ordering and the spin-glass state coexist at low temperatures. The coexistence of long-range collinear antiferromagnetic ordering and a glassy state has been reported in systems
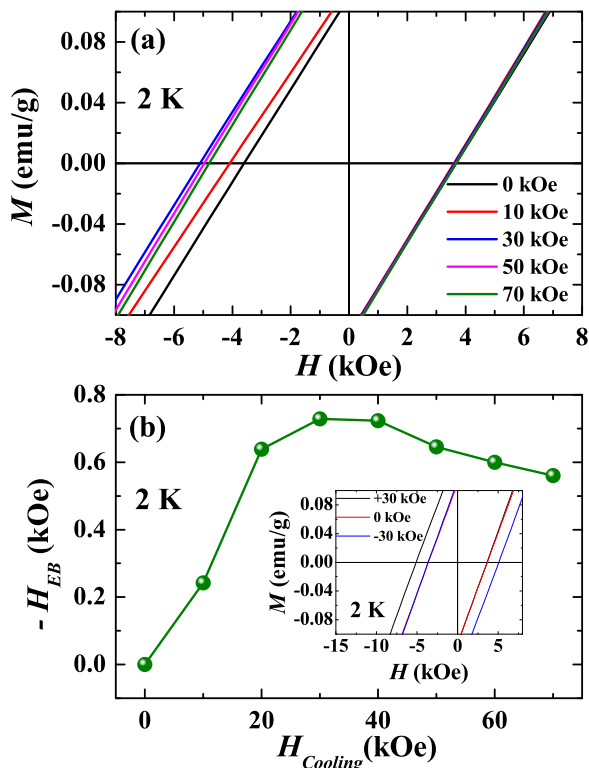
FIG. 6. (Color online) (a) Field-cooled isothermal magnetization measured with different cooling fields at 2 K. (b) Cooling-field-dependent negative exchange bias field ($-H_{EB}$) at 2 K. The inset shows the reversible shift of the hysteresis loop upon cooling with an opposite magnetic field of ± 30 kOe.
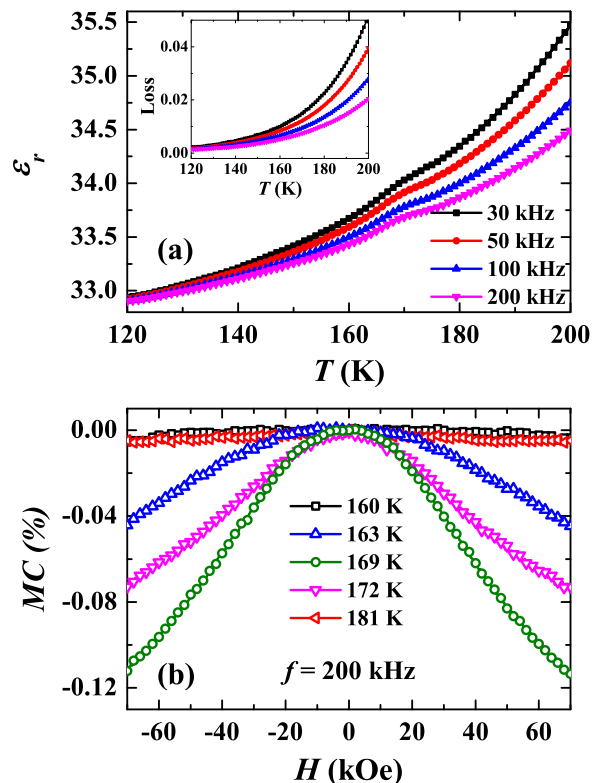

FIG. 7. (Color online) (a) Temperature-dependent dielectric constant measured with different frequencies. Temperature-dependent loss is shown in the inset. (b) Magnetic field-dependent isothermal magnetocapacitance measured at different temperatures around 170 K with 200 kHz frequency.

such as $Fe_{0.55}Mg_{0.45}Cl_2$ [43], $Fe_xMn_{1-x}TiO_3$ [44], and $PbFe_{0.5}Nb_{0.5}O_3$ [45,46]. The existence of a glassy state in the present compound is consistent with the complex crystal structure and disordered arrangement of Fe^{3+} and Mn^{3+} ions in two different crystallographic sites, as discussed in detail in Ref. [13]. This disordered arrangement of Fe^{3+} and Mn^{3+} ions does not destroy the spiral ordering in the glassy state. It is important to note that long-range spiral magnetic ordering coexists with the spin-glass state, which is seldom observed. Further, since the ordered magnetic moment of the two sites of Fe^{3+}/Mn^{3+} ions increases continuously down to 7 K, as discussed in Ref. [12], it is possible that the glassy state and spiral ordering develop almost independently. However, for a more detailed microscopic origin of this mixed state, further investigation is required.

D. Exchange bias

From the coexistence of glassy and long-range ordered states, one can also expect an exchange bias effect in this system originating from the interface between the long-range antiferromagnetic (AFM) ordered phase and spin clusters. Field-cooled isothermal magnetization at 2 K with different cooling fields is shown in Fig. 6(a). It is evident from this figure that the hysteresis loops shift asymmetrically along the field axis in the direction opposite to the applied magnetic field direction upon field cooling. The shift increases with increasing cooling field up to 30 kOe and then decreases above

30 kOe. In Fig. 6(b), the cooling-field-dependent exchange bias field ($-H_{EB}$) is shown. As shown in the inset of Fig. 6(b), this shift can be reversed by applying an opposite cooling field (± 30 kOe field). This indicates the presence of an exchange bias effect in the system, which further supports the coexistence of the ordered antiferromagnetic and spin-cluster glass states at low temperatures [47–49].

E. Electrical properties

Now, we discuss the results of electrical measurements on this compound. The overall behavior of the temperature dependence of the dielectric constant [14] is similar to what was reported earlier [13], except that we observe an almost frequency-independent broad anomaly in the dielectric constant around $T^* \sim 170$ K, as shown in Fig. 7(a), corroborating the magnetodielectric effect. This anomaly is suppressed with increasing applied magnetic field [14]. On the other hand, we did not observe any noticeable anomaly in the loss, which remains as low as 0.01 at 170 K [shown in the inset of Fig. 7(a)]. Isothermal magnetocapacitance measurements were carried out around the dielectric anomaly at 200 kHz by sweeping the magnetic field from $+70$ to -70 kOe, and the results are shown in Fig. 7(b). It is interesting to note the existence of magnetocapacitance around the dielectric anomaly. It is worth mentioning that a similar broad dielectric anomaly and magnetocapacitance effect have been observed in $BiMnO_3$ around
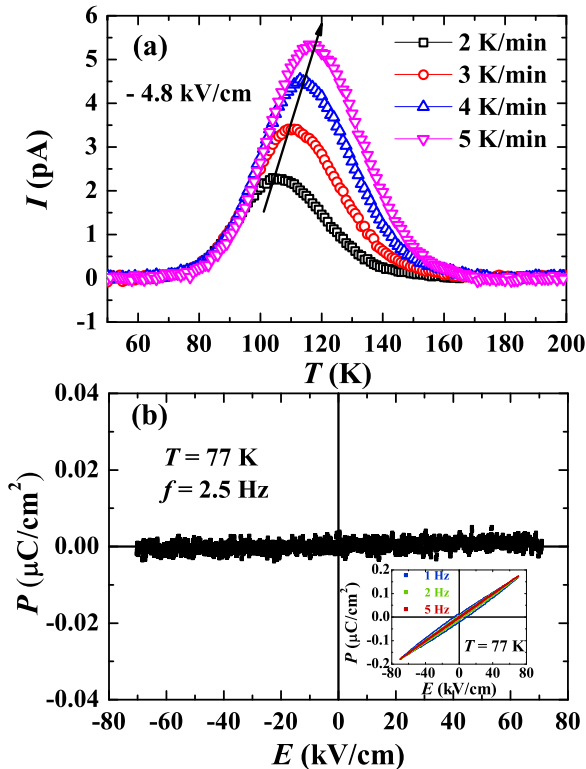
FIG. 8. (Color online) (a) Pyroelectric current measured with different heating rates with a poling field of -4.8 kV/cm. (b) P-E loop obtained from the PUND method at 77 K. The inset shows the conventional P-E hysteresis loop measured with different frequencies at 77 K.

the ferromagnetic transition temperature ($\sim$100 K), which has been attributed to the intrinsic magnetoelectric coupling between ferromagnetic and ferroelectric ordering [50]. To check whether or not this magnetocapacitance has a resistive origin, we have measured the dc electrical resistivity with a two-probe method. The resistivity is as high as $\sim$10^8 Ω m at 170 K and there is no anomaly in dc electrical resistivity around this temperature [14]. Also we did not observe any magnetoresistance effect and magneto-loss around 170 K [14]. Note that, at such a high frequency ($\sim$200 kHz), the resistive part or extrinsic effect (such as space charge, grain boundary, etc.) hardly contributes to the magnetodielectric effect, since those are mostly sensitive to a low frequency ac signal only [51]. Therefore, the observed magnetocapacitance values should be intrinsic or purely capacitive in nature. The presence of a magnetocapacitance effect is an indication of the existence of possible spin phonon coupling. However, further experiments are required to understand the origin of this magnetodielectric effect.

To know whether or not this dielectric anomaly is related to a ferroelectric transition, we have measured the pyroelectric

current. It is interesting to note that a pyrocurrent peak was observed with the onset around the dielectric anomaly. Since the pyroelectric current in a polycrystalline sample may manifest other effects, such as leakage and space charge due to an electric field poling, we have performed the pyroelectric current measurements with different warming rates. We observe that with an increasing warming rate, the pyroelectric current peak shifts to high temperature, as shown in Fig. 8(a). This indicates that the pyroelectric current peak originates from a thermally stimulated depolarization current [52] and cannot be attributed to a ferroelectric transition. To further confirm the absence of ferroelectricity, we have performed conventional P-E loop and PUND measurements at 77 and 170 K. The hysteresis loop obtained from the conventional P-E loop measurements shows leaky behavior at 77 K [inset of Fig. 8(b)]. As shown in Fig. 8(b), the P-E loop obtained from the PUND method does not show any ferroelectric component at 77 K. Similar behaviors of the P-E loop were observed at 170 K. These results confirm that the magnetic anomaly, dielectric anomaly, and pyroelectric current peak are not associated with a ferroelectric transition.

IV. CONCLUSION

In conclusion, our studies show the presence of a reentrant spin-glass state at low temperatures in the complex oxide $BiMnFe_2O_6$. The interesting aspect of this work is the observation of the coexistence of long-range spiral antiferromagnetic ordering and a spin-glass state. This behavior results from the complex crystal structure and disordered arrangement of Fe^{3+}/Mn^{3+} spins in two different crystallographic sites. The dependency of irreversibility temperature (T_{irr}) and peak position (T_P) on magnetic field follow AT and GT lines, respectively. An analysis of magnetization relaxation and ac susceptibility data reveal the presence of small spin clustering in the glassy state. The observation of magnetic and dielectric anomalies at 170 K indicates the presence of a magnetodielectric effect. Isothermal magnetocapacitance measurements at sufficiently high frequency reveal the presence of a significant intrinsic magnetocapacitance effect. However, these anomalies do not indicate ferroelectricity.

[1] W. Cheong and M. Mostovoy, Nat. Mater. **6**, 13 (2007).

[2] T. Kimura, Annu. Rev. Mater. Res. **37**, 387 (2007).

[3] Y. Tokura and S. Seki, Adv. Mater. **22**, 1554 (2010).

[4] T. Kimura, Annu. Rev. Condens. Matter Phys. **3**, 93 (2012).

[5] T. Kimura, T. Goto, H. Shintani, K. Ishizaka, T. Arima, and Y. Tokura, Nature (London) **426**, 55 (2003).

[6] T. Kimura, Y. Sekio, H. Nakamura, T. Siegrist, and A. P. Ramirez, Nat. Mater. **7**, 291 (2008).

[7] K. Taniguchi, N. Abe, T. Takenobu, Y. Iwasa, and T. Arima, Phys. Rev. Lett. **97**, 097203 (2006).

[8] G. Lawes, A. B. Harris, T. Kimura, N. Rogado, R. J. Cava, A. Aharony, O. Entin-Wohlman, T. Yildirim, M. Kenzelmann, C. Broholm, and A. P. Ramirez, Phys. Rev. Lett. **95**, 087205 (2005).

[9] H. Katsura, N. Nagaosa, and A. V. Balatsky, Phys. Rev. Lett. **95**, 057205 (2005).

[10] Y. Yamasaki, S. Miyasaka, Y. Kaneko, J. P. He, T. Arima, and Y. Tokura, Phys. Rev. Lett. **96**, 207204 (2006).

[11] S. Ishiwata, Y. Taguchi, H. Murakawa, Y. Onose, and Y. Tokura, Science **319**, 1643 (2008).

[12] A. M. Abakumov, A. A. Tsirlin, J. M. Perez-Mato, V. Petříček, H. Rosner, T. Yang, and M. Greenblatt, Phys. Rev. B **83**, 214402 (2011).

[13] T. Yang, A. M. Abakumov, J. Hadermann, G. Van Tendeloo, I. Nowik, P. W. Stephens, J. Hemberger, A. A. Tsirlin, K. V. Ramanujachary, S. Lofland, M. Croft, A. Ignatov, J. Sun, and M. Greenblatt, Chem. Sci. **1**, 751 (2010).

[14] See Supplemental Material at http://link.aps.org/supplemental/10.1103/PhysRevB.90.024413 for powder x-ray diffraction pattern, deviation of AT line at high field, dielectric and resistivity data.

[15] H. Rietveld, J. Appl. Crystallogr. **2**, 65 (1969).

[16] J. Rodriguez-Carvajal, "FULLPROF: A program for Rietveld refinement and pattern matching analysis," Abstracts of the Satellite Meeting on Powder Diffraction of the XV Congress of the IUCr. Toulouse, France, 1990, p. 127 (unpublished).

[17] M. Fukunaga and Y. Noda, J. Phys. Soc. Jpn. **77**, 064706 (2008).

[18] C. De, T. H. Kim, K. H. Kim, and A. Sundaresan, Phys. Chem. Chem. Phys. **16**, 5407 (2014).

[19] A. P. Ramirez, Annu. Rev. Mater. Sci. **24**, 453 (1994).

[20] J. R. L. de Almeida and D. J. Thouless, J. Phys. A: Math. Gen. **11**, 983 (1978).

[21] M. Gabay and G. Toulouse, Phys. Rev. Lett. **47**, 201 (1981).

[22] N. Khan, A. Midya, P. Mandal, and D. Prabhakaran, J. Appl. Phys. **113**, 183909 (2013).

[23] Z. Fu, Y. Zheng, Y. Xiao, S. Bedanta, A. Senyshyn, G. G. Simeoni, Y. Su, U. Rücker, P. Kögerler, and T. Brückel, Phys. Rev. B **87**, 214406 (2013).

[24] J. Lago, S. J. Blundell, A. Eguia, M. Jansen, and T. Rojo, Phys. Rev. B **86**, 064412 (2012).

[25] K. S. Manoj, S. K. Ram, W. Prellier, and J. F. Scott, J. Phys.: Condens. Matter **21**, 042202 (2009).

[26] S. Chatterjee and A. K. Nigam, Phys. Rev. B **66**, 104403 (2002).

[27] J. A. Mydosh, *Spin Glasses: An Experimental Introduction*, Vol. 125 (Taylor & Francis, London, 1993).

[28] P. C. Hohenberg and B. I. Halperin, Rev. Mod. Phys. **49**, 435 (1977).

[29] K. Binder and A. P. Young, Rev. Mod. Phys. **58**, 801 (1986).

[30] A. Malinowski, V. L. Bezusyy, R. Minikayev, P. Dziawa, Y. Syryanyy, and M. Sawicki, Phys. Rev. B **84**, 024409 (2011).

[31] R. Mathieu, M. Hudl, and P. Nordblad, Europhys. Lett. **90**, 67003 (2010).

[32] K. Jonason, E. Vincent, J. Hammann, J. P. Bouchaud, and P. Nordblad, Phys. Rev. Lett. **81**, 3243 (1998).

[33] P. Koželj, S. Jazbec, S. Vrtnik, A. Jelen, J. Dolinšek, M. Jagodič, Z. Jagličić, P. Boulet, M. C. de Weerd, J. Ledieu, J. M. Dubois, and V. Fournée, Phys. Rev. B **88**, 214202 (2013).

[34] D. Choudhury, P. Mandal, R. Mathieu, A. Hazarika, S. Rajan, A. Sundaresan, U. V. Waghmare, R. Knut, O. Karis, P. Nordblad, and D. D. Sarma, Phys. Rev. Lett. **108**, 127201 (2012).

[35] A. Bhattacharyya, S. Giri, and S. Majumdar, Phys. Rev. B **83**, 134427 (2011).

[36] S. Chattopadhyay, S. Giri, and S. Majumdar, Europhys. Lett. **98**, 27004 (2012).

[37] R. S. Freitas, L. Ghivelder, F. Damay, F. Dias, and L. F. Cohen, Phys. Rev. B **64**, 144404 (2001).

[38] R. V. Chamberlin, J. Appl. Phys. **57**, 3377 (1985).

[39] M. Ulrich, J. García-Otero, J. Rivas, and A. Bunde, Phys. Rev. B **67**, 024416 (2003).

[40] F. Rivadulla, M. A. López-Quintela, and J. Rivas, Phys. Rev. Lett. **93**, 167206 (2004).

[41] Y.-k. Tang, Y. Sun, and Z.-h. Cheng, Phys. Rev. B **73**, 012409 (2006).

[42] M. Kaustuv, D. Samal, A. K. Bera, E. Suja, S. M. Yusuf, and P. S. A. Kumar, J. Phys.: Condens. Matter **26**, 016002 (2014).

[43] P.-z. Wong, S. von Molnar, T. T. M. Palstra, J. A. Mydosh, H. Yoshizawa, S. M. Shapiro, and A. Ito, Phys. Rev. Lett. **55**, 2043 (1985).

[44] H. Yoshizawa, S. Mitsuda, H. Aruga, and A. Ito, Phys. Rev. Lett. **59**, 2364 (1987).

[45] G. M. Rotaru, B. Roessli, A. Amato, S. N. Gvasaliya, C. Mudry, S. G. Lushnikov, and T. A. Shaplygina, Phys. Rev. B **79**, 184430 (2009).

[46] W. Kleemann, V. V. Shvartsman, P. Borisov, and A. Kania, Phys. Rev. Lett. **105**, 257202 (2010).

[47] S. Karmakar, S. Taran, E. Bose, B. K. Chaudhuri, C. P. Sun, C. L. Huang, and H. D. Yang, Phys. Rev. B **77**, 144409 (2008).

[48] S. K. Giri, A. Poddar, and T. K. Nath, AIP Adv. **1**, 032110 (2011).

[49] M. Ali, P. Adie, C. H. Marrows, D. Greig, B. J. Hickey, and R. L. Stamps, Nat. Mater. **6**, 70 (2007).

[50] T. Kimura, S. Kawamoto, I. Yamada, M. Azuma, M. Takano, and Y. Tokura, Phys. Rev. B **67**, 180401 (2003).

[51] G. Catalan, Appl. Phys. Lett. **88**, 102902 (2006).

[52] Y. Kohara, Y. Yamasaki, Y. Onose, and Y. Tokura, Phys. Rev. B **82**, 104419 (2010).